Cancer Nanotechnology

RESEARCH Open Access

HB5 aptamer-tagged graphene oxide for co-delivery of doxorubicin and silibinin, and highly effective combination therapy in breast cancer

Maryamsadat Shahidi[1], Bibi Fatemeh Haghiralsadat[2], Omid Abazari[1], Mahdie Hemati[2,3], Parisa Dayati[4], Hossein Zarei Jaliani[5], Najmeh Sadat Hosseini Motlagh[6], Seyed Morteza Naghib[7] and Ali Moradi[1*]

*Correspondence: morady2008@gmail.com

[1] Department of Clinical Biochemistry, School of Medicine, Shahid Sadoughi University of Medical Sciences and Health Services, Yazd, Iran
[2] Medical Nanotechnology and Tissue Engineering Research Center, Yazd Reproductive Sciences Institute, Shahid Sadoughi University of Medical Sciences, Yazd, Iran
[3] Department of Clinical Biochemistry, Faculty of Medicine, Shahid Sadoughi University of Medical Sciences, Yazd, Iran
[4] Department of Clinical Biochemistry, Faculty of Medical Sciences, Tarbiat Modares University, Tehran, Iran
[5] Department of Medical Biotechnology, School of Medicine, Shahid Sadoughi University of Medical Sciences, Yazd, Iran
[6] Department of Biomedical Engineering, Meybod University, Meybod, Iran
[7] Nanotechnology Department, School of Advanced Technologies, Iran University of Science and Technology and Biomaterials and Tissue Engineering Department, Breast Cancer Research Center, Motamed Cancer Institute, IUST, ACECR, Tehran, Iran

Abstract

Using a chemotherapeutic agent, such as doxorubicin (DOX), with a natural agent, such as silibinin (Sili), is highly valuable to minimize systemic toxicity. However, Sili and DOX face disadvantages, such as low aqueous solubility and poor bioavailability. Here, we have engineered a drug delivery cargo by decorating carboxylated graphene oxide (cGO) with an aptamer, HB5, for simultaneous delivery of DOX and Sili as a combination therapy against MCF-7 and SK-BR-3 breast cancer cells. The resulting Apt-cGO displayed a typical sheet-like nanostructure with a broad surface. The maximum entrapment efficiency was 70.42% and 84.22% for Sili and DOX, respectively. When the Apt-cGO-DOX-Sili nanocomposites were selectively taken up by breast cancer cells, the interaction between cGO and drugs was cleaved, causing releasing both Sili and DOX into the tumor cells, respectively. Compared to free drugs, Apt-cGO-DOX-Sili nanocomposites displayed higher cytotoxicity in vitro. Apt-cGO-DOX-Sili nanocomposites potentially suppressed some cancer cell survival signals. They accelerated cell apoptosis and increased Rb levels as well as reduced Akt, mTOR, NF-κB, and CDK2 levels. In conclusion, the developed Apt-cGO-DOX-Sili can be suggested as a simple and efficient drug delivery approach for breast chemotherapy.

Keywords: Breast cancer therapy, Silibinin, Doxorubicin, Nanoparticles, Graphene oxide

Introduction

Female breast cancer is the most prevalent cancer worldwide, with over 2.3 million new cases in 2020 (Sung et al. 2021). Despite recent advances in treating breast cancer, chemotherapy remains the primary treatment option in clinical practice (Senapati et al. 2018). Conventional chemotherapeutic agents mainly interfere with DNA replication and cell division, leading to the death of rapidly growing tumor cells (Yan et al. 2020). Nonetheless, these drugs encounter challenges, such as a lack of sufficient targeting ability, poor

biocompatibility, limited bioavailability, and the development of drug resistance (Afzal et al. 2021).

Doxorubicin (DOX, $C_{27}H_{29}NO_{11}$) was extensively employed as the first-line chemotherapeutic agent to treat a broad spectrum of human cancers for a long time. One of the main anticancer mechanisms of DOX is inhibiting topoisomerase II and subsequently stopping DNA replication. Another suggested mechanism by which DOX acts in the tumor cell is the generation of free radicals, which might generate oxidative stress, resulting in DNA damage and cell death (van der Zanden et al. 2021). Previous studies on various cancer cell models proposed that DOX play a fundamental role in modulating some cellular processes, including apoptosis promotion and cell cycle arrest (Chen et al. 2015). Despite the extensive clinical utilization of DOX, its efficacy is restricted due to wide serious toxicity on healthy tissues and drug resistance (Varela-López et al. 2019). Recently, effective strategies have been widely developed to overcome DOX resistance and reduce its side effects (Firouzi Amoodizaj et al. 2020).

In recent years, combination chemotherapy has gained much attention that can raise the therapeutic index of clinical chemotherapeutic drugs. In this regard, numerous phytochemical products have been suggested and studied due to their anticancer activities as ideal candidates for combination chemotherapy. Many researchers have proposed that the combination of DOX together with a phytochemical product with a known mechanism of action might generate synergistic anticancer effects and maximize its therapeutic effectiveness (Liu et al. 2020). Silibinin (Sili, $C_{25}H_{22}O_{10}$) is a major active constituent purified from the seeds of the milk thistle (Silybum marianum); it is explored on a broad range of therapeutic activities, including anti-inflammatory, antioxidant, and anticancer properties (Tuli et al. 2021; Karimi et al. 2022). In a prior study, treatment with Sili strongly reduced the viability of HepG2 cells and synergized the therapeutic effect of DOX in hepatocellular carcinoma (HCC) through inducing cell apoptosis and G2-M arrest (Li and Wang 2016). In addition, Sili has revealed minimal or no apparent side effects in human except gastrointestinal disorders (Ghalehkhondabi et al. 2021). Another anticancer mechanism of Sili is the regulation of multiple dominant pathways in tumor cells, and in particular, nuclear factor kappa B (NF-κB) signaling, extracellular signal-regulated kinase signaling (ERK), and protein kinase B signaling (Akt) (Si et al. 2019; Pourgholi et al. 2021). Accordingly, combination therapy using Sili and DOX may also exhibit a better therapeutic result against breast cancer.

Despite these beneficial therapeutic effects, Sili and DOX are hydrophobic agents with poor bioavailability (Pooja et al. 2014). Different strategies have been proposed to intensify their bioavailability, including complexation with water-soluble derivatives (Nawaz et al. 2020; Chandra et al. 2020). Nanoencapsulation of hydrophobic drugs represents various advantages, including low toxicity, long-term stability, targeted drug delivery, and controlled/sustained drug release (Patra et al. 2018). Over the last decade, graphene derivatives-based nanomaterials have attracted great attention due to their unique features, such as good solubility, high biocompatibility, and surface functionalization ability (Dasari Shareena et al. 2018). Graphene is an allotrope of carbon with a two-dimensional honeycomb lattice structure (hexagonal lattice); its derivatives can be effectively employed for drug delivery (Song et al. 2020). Graphene oxide (GO) is introduced as an attractive structure in biomedical studies due to its

broad surface area and functional groups, which provide the possible attachment of targeting molecules. However, GO materials are highly acidic, which could damage healthy cells, thus jeopardizing their function as a drug delivery platform (Esmaeili et al. 2020). In the current study, the carboxylate graphene oxide (cGO) is developed as a cargo system to improve the poor biopharmaceutical properties and limit the aqueous solubility of Sili and DOX. Based on previous studies, cGO is highly biocompatible with healthy cells, suggesting that it is suitable for the drug delivery (Gholami et al. 2020).

It was declared that the targeted delivery of nanocomposites could be a promising strategy to transport chemotherapeutic agents to the target cells selectively and minimize the undesired effects (Yi et al. 2018; Shahidi et al. 2022b; Shahidi et al. 2022a). Human epidermal growth factor receptor 2 (HER2) is a 185-kDa transmembrane oncoprotein highly expressed in nearly 25% of invasive breast cancers (Subramaniyan et al. 2022). Growing evidence cleared that a newly developed DNA aptamer (HB5) binds specifically to the HER2-positive breast cancer cells, suggesting that HB5-tagged nanoparticles could be selectively taken up by cancer cells and minimize the side effects of chemotherapeutic drugs (Wu et al. 2017; Liu et al. 2012). According to this view, HB5 aptamer was covalently attached to our novel-designed cGO to enhance cellular internalization. Until now, the targeted co-delivery of DOX and Sili using HB5-cGO nano complex to breast cancer cells is not described in the literature. Therefore, we engineered Apt-cGO-DOX-Sili nanocomposites to simultaneously deliver DOX and Sili and explore their efficacy on breast cancer in vitro (Fig. 1).

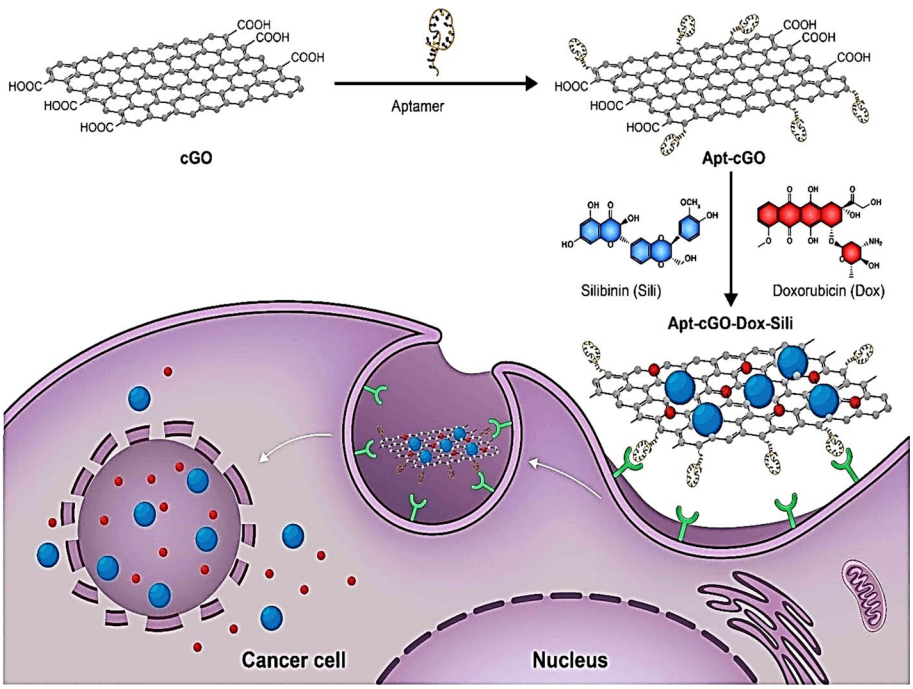

Fig. 1 Representative image of drug delivery system. cGO: carboxylated graphene oxide; Apt: aptamer; DOX: doxorubicin; Sili: silibinin

Materials and methods

Synthesis of GO

Synthesis of GO was conducted through Hummers' method with a slight modification (Hummers and Offeman 1958). In detail, 3 g graphite flakes (Sigma-Aldrich; USA) were dissolute gradually in a 9:1 mixture containing concentrated H2SO4 (360 mL) and H3PO4 (40 mL) under 15 min of stirring. Subsequently, 18 g potassium permanganate (KMnO4, Sigma-Aldrich; USA) was slowly added to the mixture under vigorous stirring. Using a temperature-controlled water bath, the solution was heated for 1 h under stirring to produce a slight exotherm reaction (35–40 °C) and avoid overheating. Subsequently, the solution was stirred at a higher temperature (50 °C) for another 12 h. Then, 400 mL of ice-sterile deionized water and 3 mL of 30% H_2O_2 (3 mL) were gradually supplemented to remove excess KMnO4 and stop the oxidation (Song et al. 2022). Afterward, the resultant solution was centrifuged at 4000 rpm for 4 h. The supernatant was discarded, and the precipitated material was rinsed twice with 30% HCl (200 mL) and five times with ultrapure deionized water (200 mL), followed by centrifugation (4000 rpm for 4 h). The resulting suspension was filtered, and the solid substance was dried under vacuum at 25 °C overnight to obtain the purified GO powder.

Preparation of cGO

In brief, 0.072 g of sodium hydroxide (NaOH; 40 g/mol) was added to 2 mL of a GO (2 mg/mL) and the mixture was sonicated for 4 h at room temperature. After that, the solution was mixed with 0.4 mL of HCl (37% v/v). The mixture was rinsed with deionized water and centrifugated at 9000 rpm for 5 min to remove its salts (Motlagh et al. 2020). The final mixture was purified by repeated rinsing and centrifugation. Finally, the product was lyophilized to give the cGO black powder of interest.

Conjugation of Apt to cGO

HB5 aptamer for HER2-positive cancer cells was previously reported as the targeting ligand (Liu et al. 2012). The sequence of the aptamer ($n=60$) was 5′-(AACCGC CCAAATC(dNP)nCTACACACCCACA)-3. Apt was tagged on the surface of cGO nanosheets by a classical amide bond formation between –COOH groups of cGO and –NH2 groups of modified Apt. In detail, 10 mg cGO, 10 mg of 1-ethyl-3-(3-dimethyl aminopropyl)-carbodiimide (EDC; Sigma-Aldrich; USA), and 0.0175 mg of *N*-hydroxysuccinimide (NHS; Sigma-Aldrich; USA) was dissolved in 2 mL distal water and stirred for 1 h. Afterward, 6 µL of Apt solution (1 µM stock solution) was added to the suspension, and the mixture was stirred at ambient temperature for 20 h. The final solution was centrifuged (3000 rpm; 5 min), rinsed three times with deionized water, and then freeze-dried for 48 h to obtain Apt-cGO.

Drug loading on the cGO surface

In brief, 250 µg of DOX (dissolved in 1 mL PBS) (Sigma-Aldrich; USA) was mixed with 400 µg of cGO or Apt-cGO (dispersed in 1 mL PBS) and stirred for 48 h at room temperature. For Sili loading, 450 µg of Sili (dissolved in 700 µL PBS + 300

μL dimethyl sulfoxide) (DMSO; Sigma-Aldrich; USA) was mixed with 400 μg cGO or Apt-cGO (dispersed in 1 mL PBS) and stirred for 48 h at room temperature. For loading two drugs, Sili and DOX with a 1:1 ratio were simultaneously added to 400 μg/mL of Apt-cGO and stirred for 48 h at room temperature. After centrifugation (13,000 rpm for 10 min), the supernatant (unbounded Sili and DOX) was collected, and the pelleted substance was re-suspended in PBS solution. The amount of free Sili and DOX was assessed by NanoDrop spectrophotometer equipment (Epoch BioTek, USA) at 287 and 480 nm, respectively. Ultimately, the entrapment efficiency (EE%) and loading efficiency (LE%) of each drug were measured using its standard chart according to the following formula:

$$\mathrm{EE\%} = \frac{\text{Total amount of drug} - \text{Free drug}}{\text{Total amount of drug}} \times 100$$

$$\mathrm{LE\%} = \frac{\text{Total amount of drug} - \text{Free drug}}{\text{NPs Mass}} \times 100$$

Characterizations of nanocarrier

The structures of cGO and Apt-cGO were determined by Field Emission Scanning Electron Microscope (FE-SEM; model EM3200, KYKY, China) and Atomic Force Microscopy (AFM; model: Nano Wizard®II NanoScience AFM, JPK Instruments Inc., Germany). The molecular structure of the cGO, Apt-cGO, Apt-cGO-DOX, and Apt-cGO-Sili was evaluated using Fourier transform infrared spectroscopy (FTIR; Bruker Tensor 27) by mixing the nanostructures in potassium bromide (KBr) pellets and was recorded at 4000–400 cm^{-1} wavenumber range. The particle size, polydispersity index (PDI), and surface charge of different formulations was estimated using dynamic light scattering (DLS) by a Zetasizer instrument (Horbia Jobin Jyovin) in each fabrication step. In each synthesis step, the absorption peaks of nanostructures were determined by UV–visible spectrophotometry (UV–Vis; Epoch Box 998 America) absorption spectra.

The electrostatic adsorption of aptamer onto cGO was also investigated using an agarose gel retardation assay. Free aptamer (positive control) and Apt-cGO nanocomposites were mixed in a total volume of 10 μL in PBS and run on 2% (w/v) agarose gel at a voltage of 120 V for 1 h.

Drug release assay

The release profiles of Sili and DOX from cGO or Apt-cGO were determined using a 12 kDa cutoff dialysis membrane (Sigma-Aldrich; USA). In brief, cGO-DOX-Sili and Apt-cGO-DOX-Sili were separately re-suspended into 500 μL of PBS solution (pH 7.4 and pH 5.5) and transferred into a dialysis bag. It was then placed in a water bath at 37 °C and 42 °C under continuous gentle agitation at predetermined intervals (0, 2, 4, 6, 12, 18, 24, 48, and 72 h). About 0.5 mL of PBS buffer was withdrawn and replaced with an equal volume of fresh buffer. The amount of released DOX and Sili was investigated by recording their absorbance by the UV–Vis spectrophotometer at 287 and 480 nm. The drug release percentages were determined according to the standard curve of Sili and DOX in PBS solution.

Cell culture

MCF-10A, MCF-7, and SK-BR-3 cell lines were provided from Pasteur Institute (Tehran, Iran) and grown in RPMI 1640 medium (Bioidea, Iran) with 10% fetal bovine serum (FBS; Gibco, Invitrogen, NY, USA) and penicillin (100 U/mL)–streptomycin (100 µg/mL; Bioidea, Iran) under standard conditions in a cell incubator (37 °C and 5% CO_2). All cell experiments were accomplished in the logarithmic phase of growth.

In vitro cellular uptake

To study in vitro cellular uptake of different formulations, MCF-10A, MCF-7, and SK-BR-3 cell lines (1.5×10^5 cells/well) were planted in a 24-well plate for 24 h and then exposed to varying formulations for 3 h. Subsequently, the treated and untreated cells were rinsed three times with cold PBS solution (pH 7.4) and fixed with 95% ethanol solution at room temperature. The fluorescence intensity of DOX (autofluorescence), Sili (autofluorescence), and cGO (labeled with fluorescein isothiocyanate (FITC)) were visualized under fluorescence microscopy (Olympus, Japan). FITC-labeled cGO samples were prepared as previously described (Li et al. 2018). For nuclear staining, the cells were stained by 4′,6-diamidino-2-phenylindole (DAPI dye; 0.125 µg/mL) for 15 min. Finally, the cellular uptake capacity was quantified by calculating the corrected total cell fluorescence (CTCF) based on the fluorescence intensity of the images using Image J software

$$\text{CTCF} = \text{Integrated Density} - (\text{Area of selected cell} \times \text{Mean fluorescence of background})$$

Cytotoxicity assay

The cytotoxicity of free drugs and their different formulations was figured out using the 3-(4,5-dimethylthiazol-2-yl)-2,5-diphenyl tetrazolium bromide (MTT) assay (Sigma; USA). MCF-10A, MCF-7, and SK-BR-3 cells with a density 10^4 cells/well were planted into 96-well plates for 24 h, and then exposed to bare cGO (5, 10, 20, 40, 80, 160, 320, 640, and 1280 µg/mL), Apt (10, 20, 40, 80, 100, 200, 300, and 500 µg/mL), free DOX (0.002, 0.007, 0.022, 0.066, 0.2, 0.6, 1.8, 5.4, and 7.02 µg/mL), cGO-DOX (0.003, 0.011, 0.033, 0.1, 0.3, 0.9, 2.7, 8.1, and 24.3 µg/mL), Apt-cGO-DOX (0.003, 0.011, 0.033, 0.1, 0.3, 0.9, 2.7, 8.1, and 24.3 µg/mL), free Sili (2.47, 4.95, 9.9, 19.8, 39.6, 79.2, 158.4, 316.4, and 633.6 µg/mL) and cGO-Sili (0.625, 1.25, 2.5, 5, 10, 20, 40, 80, and 160 µg/mL), and cGO-DOX-Sili (0.95, 1.9, 3.9, 7.8, 15.75, 31.5, 63, 126, 252 µg/mL) and Apt-cGO-DOX-Sili (0.013, 0.04, 0.122, 0.366, 1.1, 3.29, 9.88, 29.66, and 89 µg/mL) for a period of 48 h. After this, 10 µL of MTT solution (5 mg/mL) was placed in each well, and the cells were incubated for another 3 h. Subsequently, the medium was withdrawn from each well and replaced by 100 µL of DMSO to dissolve the formazan crystals. Eventually, the optical density of samples was determined at 570 nm using an EPOCH spectrophotometer (Bio-Tek, Winooski).

$$\text{Cell viability}(\%) = \frac{\text{OD treated cells}}{\text{OD control cells}} \times 100$$

Combination index (CI)

The synergistic effects of Sili and DOX were calculated using CI by the Chou–Talalay method and CompySyn software (version 1.0). For drug combinations, CI < 1, CI = 1, and

CI > 1 were defined as synergism, additive effect, and antagonism effects, respectively (Chou 2010).

Real-time quantitative reverse transcription PCR (RT-qPCR) analysis

RT-qPCR technique was employed to compare the transcript levels of Akt, mammalian target of rapamycin (mTOR), NF-κB, cyclin dependent kinase 2 (CDK2), and retinoblastoma ((Rb) genes in the cancer cells treated with different formulations based on their IC50s. In brief, MCF-7 and SK-BR-3 cells with a density of 1.5×10^5 cells/well were planted in six-well plates for 24 h. Subsequently, the cells were treated with the formulations for 48 h. After this, total RNA isolation was done from each well using the Sinnaclon RNX Plus isolation kit (Iran), following the protocol provided by the manufacturer. Consequently, isolated total RNA molecules were converted to cDNA using the Parstous cDNA synthesis kit (Iran). Subsequently, RT-qPCR was applied using 2 × SYBR Green qPCR Mix (YektaTajhiz, Iran), cDNA template, and the specific primers on the Rotor-Gene Q thermal cycler (QIAGEN, Germany). Finally, the relative gene expression levels were analyzed using absolute threshold cycle values (Ct values) by the $2^{-\Delta\Delta CT}$ method. The primer sequences of Akt, NF-κB, mTOR, Rb, CDK2, and glyceraldehyde-3-Phosphate Dehydrogenase (GAPDH; a housekeeping gene) genes are provided in Table 1.

Western blotting assay

The western blotting technique evaluated the CDK2 and Rb protein expression levels. In detail, MCF-7 and SK-BR-3 cells were planted in 6-well plates (1.5×10^5 cells/well) and exposed to different formulations for 48 h based on their IC50s. After this, all wells were washed with PBS three times, harvested in RIPA buffer, and centrifuged at 16,000 rpm for 20 min, and subsequently, the protein content was measured using Bradford protein assay (Kruger 2009). Equal contents of the protein extracts (50 μg) were run on 10% SDS–PAGE gel and then absorbed onto a nitrocellulose membrane (Sigma; USA). The membrane was exposed to 5% bovine serum albumin (BSA, Sigma; USA) blocking buffer for 1 h at room temperature and then with primary antibodies for CDK2 (Santa Cruz, USA; 1:1000), Rb (Santa Cruz; the USA, 1:1000), and β-actin (Santa Cruz; the

Table 1 Primer's sequences utilized for RT-qPCR

Genes	Sequence
Akt	Forward: 5′-CTGCTCAAGAAGGACCCCAA-3′
	Reverse: 5′-AGGTGGTGTGATGGTGATC-3′
mTOR	Forward: 5′-CCAGGAGTTACTTCTATGCC-3′
	Reverse: 5′-GAAATCCGCTTGTTAGGGTC-3′
NF-κB	Forward: 5′-ACACCGAAGCAATTGAAGTG-3′
	Reverse: 5′-ATGGGGCATTTTGTTGAGAG-3′
CDK2	Forward: 5′-GAGCCAGCCCATAAGAAAAC-3′
	Reverse: 5′-CACCAGCCAATATAGCACTG-3′
Rb	Forward: 5′-GAATCATTCGGGACTTCTG-3′
	Reverse: 5′-TCTGCTTCATCTGATCCTTC-3′
GAPDH	Forward: 5′-CAAGTTCAACGGCACAGTCAAG-3′
	Reverse: 5′-CATACTCAGCACCAGCATCACC-3′

USA, 1:1000) at 4 °C overnight, followed by horseradish peroxidase-labeled anti-rabbit secondary antibodies (1:2000) at room temperature for 1 h. Finally, the membranes were visualized and analyzed with an electrochemiluminescence (ECL) detection reagent (GE Healthcare) and Image J software.

Apoptosis analysis

Briefly, MCF-7 and SK-BR-3 cells (1.5×10^5 cells/well) were planted in six-well plates for 24 h and then exposed to different formulations for 24 h based on their IC50s. Subsequently, breast cancer cells were collected, re-suspended in the binding buffer, and stained with Annexin V-FITC/propidium iodide (PI) dye solution for 15 min following the manufacturer's instructions (Abcam; Cambridge; UK). Eventually, the apoptosis rate of cancer cells was evaluated using a flow cytometer (Roche; Germany) and analyzed by Flowjo™ V10 software.

Statistical analysis

The measurement of statistical difference was determined by Student's *t* test and one-way analysis of variance (ANOVA) using GraphPad Prism version 8 (GraphPad, San Diego, CA). The analyzed data were presented as the mean ± standard deviation (SD). p value < 0.05 was considered as a difference.

Results and discussion

Characterization of cGO and Apt-cGO nanocomposites

In the current study, HB5-tagged cGO was developed as a nanocarrier for transporting Sili and DOX to breast cancer cells. At first, the uniformly GO sheets were successfully produced from the graphite flakes according to the modified Hummers' method and then carboxylated to yield cGO (Malik et al. 2015; Alibolandi et al. 2017). During the oxidation process, C═C double bonds break down, and oxygen-containing groups, such as carboxylic acid (–COOH), hydroxyl (–OH), and epoxy (C–O–C), are distributed on GO sheets (Ghulam et al. 2022). Under the strongly alkaline condition, the hydroxyl functional groups are further converted to carboxylic acid moieties (Guo et al. 2020). Subsequently, HB5 aptamer was attached to the surface of cGO through the amide reaction between the carboxyl groups of cGO and the amine groups of the modified aptamer. This drug delivery system was first characterized using various spectroscopy and microscopy techniques. Morphological analysis was accomplished using FE-SEM and AFM techniques to ascertain the surface structure of bare cGO and Apt-cGO. The FE-SEM photographs of cGO particles displayed a typical sheet-like nanostructure with a broad surface. Figure 2A, andB shows that the surface of cGO was relatively flat. At the same time, the Apt-cGO had wrinkles and irregular structures, suggesting the possible anchoring of aptamers on the surface of cGO nanosheets. Besides, the AFM technique was also conducted to provide more detailed information on cGO nanosheets before and after the aptamer immobilization on the cGO sheets' surface. Figure 3A exhibits the morphology of the bare cGO surface with a Root-Mean-Squared (RMS) roughness of 1.84 nm. After anchoring aptamer molecules, the RMS roughness was raised to 4.6 nm (Fig. 3B). The results were in agreement with the previous reports. Tan et al. found that the thickness of GO sheets was raised after the Apt anchoring (Tan et al. 2018).

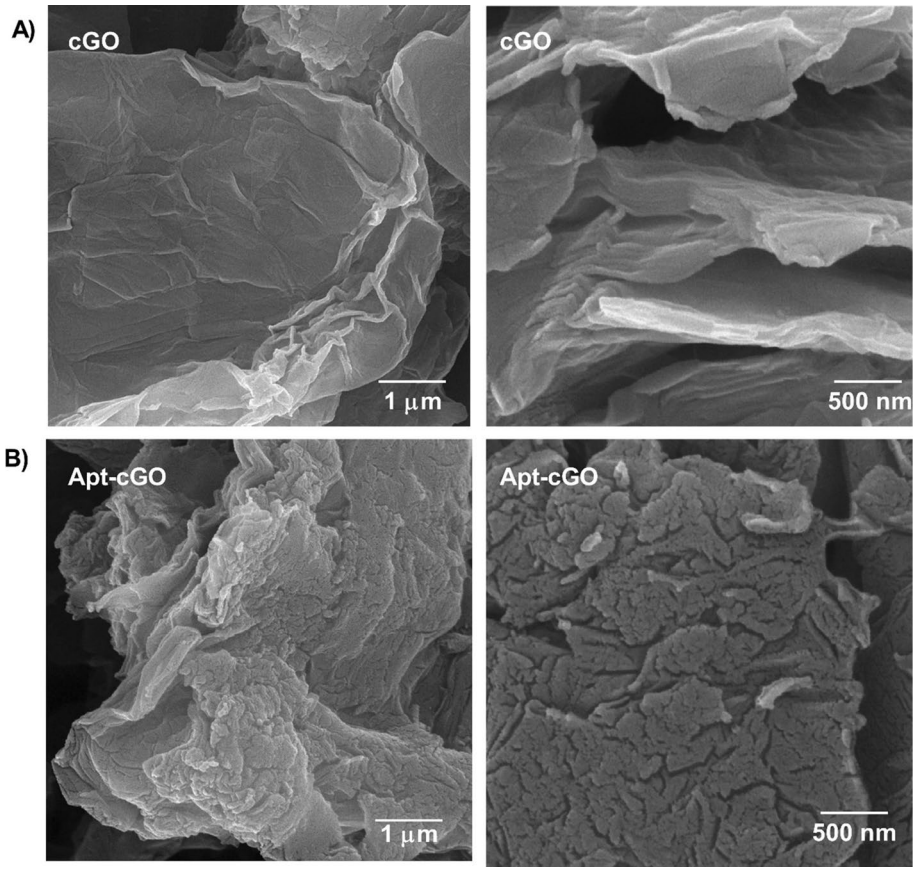

Fig. 2 FE-SEM images of cGO (**A**) and cGO-aptamer (**B**). cGO: carboxylated graphene oxide; Apt: aptamer; FE-SEM: field emission scanning electron microscopy

To better determine of nanoparticle size, DLS technique was employed. DLS estimates the particle size, PDI, and zeta potential of different formulations. The obtained cGO had the value of 160.7 ± 5.3 nm. This suitable size value is a key property of nanoparticle, because many its properties are size dependent (Shrestha et al. 2020). DLS also measures the PDI, which shows the width of the particle size distribution. The value of 0.033 ± 0.0001 indicated that cGO had a narrow particle size distribution. The value of zeta potential is considered a measurable indicator of the physical stability of nanoparticles in a colloidal suspension. A specific zeta potential amount more positive than $+30$ mV and negative than -30 mV generally reveals a desirable physical colloidal nanosuspension stability. On the other hand, a zeta potential value within $+30$ to -30 mV can result in particle aggregation and physical instability (Ali et al. 2018). In the current work, the zeta potential of cGO and Apt-cGO is provided in Fig. 3C. The negative charge of cGO (-41.75 ± 2.01 mV) was due to the presence of COOH groups on the surface of cGO sheets. When HB5 aptamers were gradually added, the zeta potential was enhanced from -41.75 ± 2.01 mV to -34.9 ± 0.9 mV, exhibiting the construction of Apt-cGO. These findings followed the results of Tan et al. They found that the zeta potential of GO was increased when the GO interacted with Apt (Tan et al. 2018).

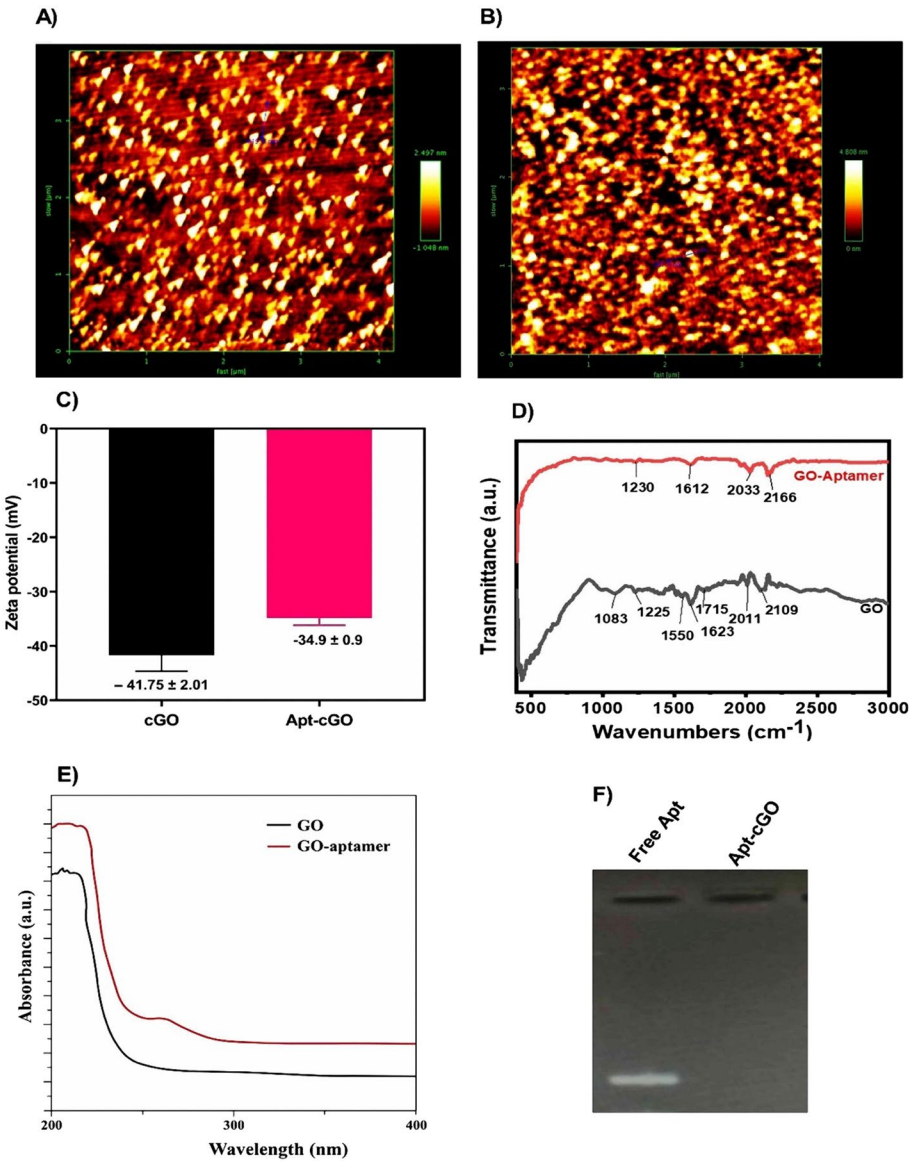

Fig. 3 AFM images (**A**, **B**), zeta potential values (**C**), FTIR spectroscopy measurements (**D**), and UV–Vis spectral absorbance (**E**) of cGO and cGO-aptamer. **F** Agarose gel electrophoresis confirmed the successful HB5 absorption on the cGO surface. AFM: atomic force microscope; FTIR: Fourier transform infrared; UV–Vis: Ultraviolet–visible; cGO: carboxylated Graphene oxide; Apt: aptamer

The FT-IR measurement and UV–Vis spectroscopy confirmed the successful immobilization of aptamers on the cGO surface. Ma et al. showed the presence of C–O–C and –COOH functional groups at 1240 cm^{-1} and 1722 cm^{-1} of the FT-IR spectrum of cGO, which was inconsistent with the cGO FT-IR spectrum in the present study (Ma et al. 2019). We exhibited the main functional groups of cGO at around 1715 cm^{-1} (C=O), 1623 cm^{-1} (C=C), 1225 cm^{-1}, and 1083 cm^{-1} (C–O). The FT-IR spectrum of Apt-cGO was almost the same as cGO. However, after conjugating with the aptamers, an amide group appeared around 1612 cm^{-1} for the N–H stretching vibration (Fig. 3D). Figure 3E represents the UV–Vis spectra of cGO and Apt-GO nanocomposites. Because of the

characteristic $\pi \rightarrow \pi^*$ molecular transition of the C=C bond in the aromatic ring, the intense absorption peak of cGO (black) was observed at 230 nm. After the immobilization of aptamer, the Apt-cGO spectrum (red) showed two absorption peaks around 230 and 260 nm. The specific absorption peak at 260 nm is related to the conjugated double bond in the purine and pyrimidine rings. These findings follow prior studies (Barbatti et al. 2012). In addition, the successful HB5 absorption was also confirmed by the agarose gel electrophoresis (Fig. 3F). After the complexation of the HB5 aptamer to cGO, the related band was not observed on the agarose gel relative to the bright band of free aptamers, proving the successful reaction between modified aptamers and cGO nanosheets. Collectively, the obtained results indicated the successful attachment of aptamer molecules on the surface of cGO for targeted drug delivery.

Characterization of dual drug-loaded nanocomposites

According to previous studies, the aromatic anticancer drugs could couple on the cGO surface via pi–pi interactions between the aromatic residues of drugs and the cGO surface (Yadav et al. 2022). In this study, the unambiguous evidence of DOX, Sili, and simultaneous attachment of DOX and Sili on the surface of cGO sheets was provided via FTIR, DLS, and UV–Vis spectroscopy analyses. As shown in Fig. 4A, the FT-IR spectrum of cGO (red) represented a broad absorption band around 3426 cm-1 (O–H). It is important to mention that this absorption band is not appeared in the FT-IR spectrum of graphite, supporting the successful construction of cGO sheets (Bustos-Ramírez et al. 2013). The characteristic peaks at 1737 cm^{-1} (C=O), 1626 cm^{-1} (C=C stretching of the GO skeleton), and 1057 cm^{-1} (C–O) have also appeared in the FT-IR spectrum of cGO. Compared to the cGO spectrum, the characteristic peak of 3426 cm^{-1} had a small shift to 3410 cm^{-1} in the cGO-DOX spectrum. The characteristic peaks at 2926 cm^{-1} (C–H), 1725 cm^{-1} (C=O), 1610 cm^{-1} (N–H), and 872 cm^{-1} (NH2) were also detected, which suggested the coupling of DOX onto cGO (Fig. 4A). According to prior studies, pure Sili FT-IR spectra exhibited the peaks at 3457, 2946, 1630, 1508, and 1269 cm^{-1} that originated from O–H, CH, C=O, C=C, and C–O–C stretching vibrations, respectively (Alipour et al. 2020; Shetty et al. 2017). In the current work, the FT-IR spectrum of cGO-Sili (blue) showed the characteristic peaks at 3434, 2932, 1639, and 1275 cm^{-1}, suggesting the presence of cGO and Sili in the cGO-Sili complex (Fig. 4A). These findings were in line with the study of Neri et al. (Shetty et al. 2017).

The zeta potential of different formulations is presented in Fig. 4B. The zeta potential value of Apt-cGO was -34.9 ± 0.9 mV, while zeta potential of DOX loaded Apt-cGO was -8.7 ± 0.9 mV, suggesting the attachment of DOX on the Apt-cGO surface. In general, DOX contains a positive surface charge due to the primary amine group, causing the more positive of Apt-cGO-DOX zeta potential compared to Apt-cGTO (Zhao et al. 2018). After Sili loading, we observed a change in the zeta potential (-28.2 ± 0.4 mV), which might be due to the good adhesion of Sili on the Apt-cGO-DOX. Extensive evidence verifies that this amount of negative charge of the nanoparticles can result in their suspension stability (Zhao et al. 2018). The size and PDI of completed formulation (Apt-cGO-DOX-Sili) was also examined. Our data showed that the size and PDI of obtained Apt-cGO-DOX-Sili were at around 200 ± 10.5 nm and 0.118 ± 0.0001, respectively.

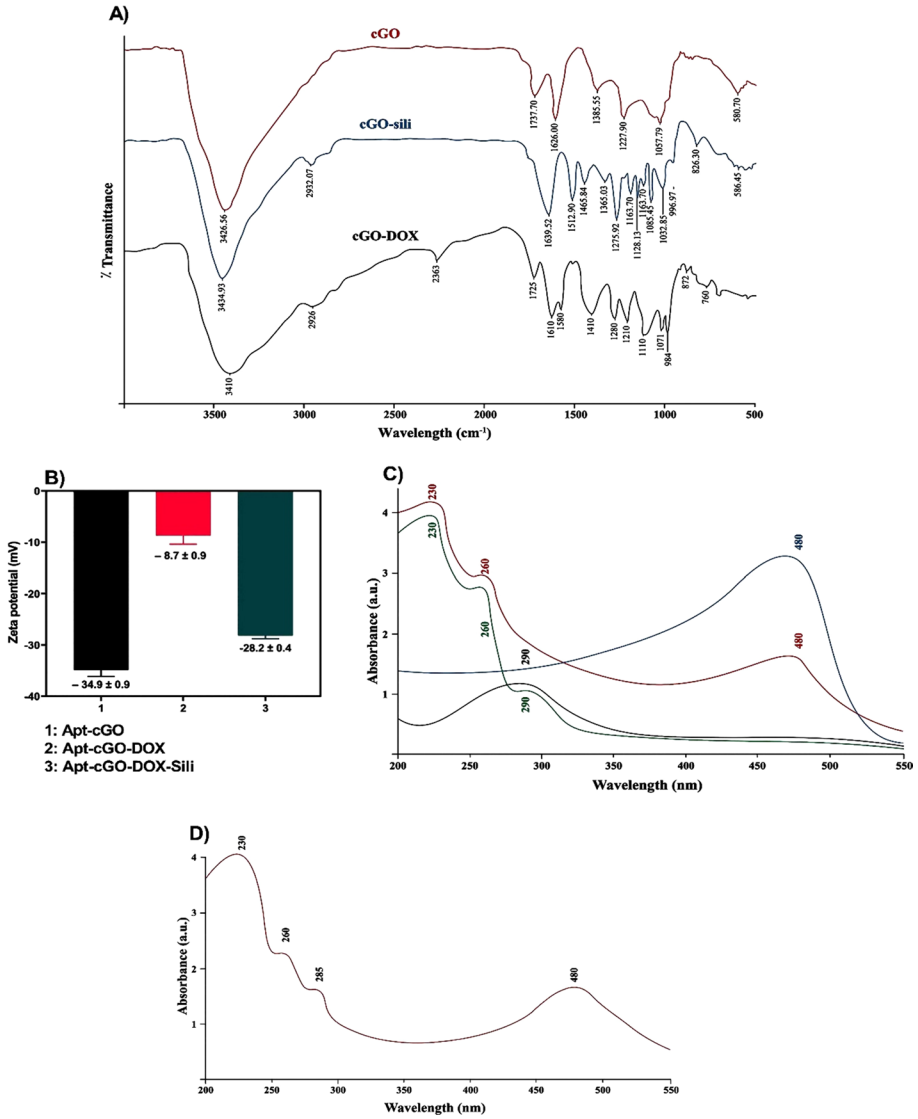

Fig. 4 **A** FT-IR cGO, cGO-DOX, and cGO-Sili. **B** Zeta potential values of Apt-cGO, Apt-cGO-DOX, and Apt-cGO-DOX-Sili formulations. **C** UV–Vis spectral absorbance of free DOX (blue), free Sili (black), Apt-cGO-DOX (red), and Apt-cGO-Sili (green). **D** UV–Vis spectral absorbance of Apt-cGO-DOX-Sili. FTIR: Fourier transform infrared; UV–Vis: Ultraviolet–visible; cGO: carboxylated graphene oxide; Apt: aptamer; DOX: doxorubicin; Sili: silibinin

As shown in Fig. 4C, the UV–Vis spectrums of free DOX and free Sili were identified by the characteristic peaks around 480 nm and 290 nm, respectively. These findings were consistent with the previous studies (Solís-Gómez et al. 2019). After DOX and Sili loading, the Apt-cGO-DOX and Apt-cGO-Sili nanocomposites exhibited new absorption peaks around 480 and 290 nm, respectively (Fig. 4C). In the simultaneous drug loading form, Apt-cGO-DOX-Sili nanocomposites exhibited four peaks around 230 nm, 260 nm, 290 nm, and 480 corresponding to cGO, Apt, Sili, and DOX, respectively (Fig. 4D).

The EE% and LE% of each drug for all formulations were also determined (Table 2). In the recent times, GO has become a desirable nanocarrier because of its high surface area and high drug loading efficiency (Pooresmaeil et al. 2020). As shown in Table 2, the

EE% and LE% of Apt-cGO-DOX-Sili reached the maximum value of 84.22% and 41.4% for DOX and 70.42% and 30.3% foe Sili NAP, respectively. However, there were no significant changes in EE% or LE% of studied formulations for DOX and Sili. Conjugation of Apt to the cGO had a negligible impact on the EE% and LE% of studied formulations.

Cellular uptake study

Although chemotherapeutic drugs have been reported to play an important role in cancer treatment, these agents themselves are non-targeted, which notably limits the drug accumulation within tumor cells and causes adverse effects toward healthy cells. Evidence from in vitro studies ascertained that a surface modification of nanoparticles with specific ligands could cause the improvement of drug content in the tumor cells (Zhu and Chen 2018). HER2 positive breast cancer is the more aggressive than some other breast cancers with low overall survival rate (Patel et al. 2020). Recently, many investigations are focused on developing aptamers for HER2 receptors for the diagnostic and therapeutic applications. Aptamer HB5 has been developed as a tumor-targeting ligand for the targeted delivery of chemotherapeutic drugs to cancer cells (Wu et al. 2017). This aptamer was able to preferentially bind to HER2-positive cells but had no affinity toward HER2-negative cells (Kim et al. 2019). For instance, Liu et al. declared that the aptamer HB5 could selectively deliver DOX to SK-BR-3 breast cancer cells, where HER-2 is highly expressed (Liu et al. 2012).

In the current work, the specificity of HB5 aptamer was evaluated for the targeted cellular entrance of the Apt-cGO nanocomposites in HER2-overexpressing SK-BR-3 cells, HER2-low expressing MCF-7 cells, and HER2-negative MCF-10A cells. Images of cellular internalization of Apt-cGO in SK-BR-3, MCF-7, and MCF-10A cell lines, which have been captured by fluorescence microscopy, are represented in Fig. 5A. DAPI and FITC were utilized for staining the nuclei and cGO, respectively. As depicted in Fig. 5A, HB5-modified cGO nanocomposites were successfully taken up by the SK-BR-3 and MCF-7 cells but not by the MCF-10A cells, indicating that HB5-modified cGO had a great targeting ability to tumor cells. These findings suggested the specific interaction between HB5-modified cGO and HER2 receptors. However, the intensity of green fluorescence of Apt-cGO in the SK-BR-3 cell line was higher than the MCF-7 cell line, due to a more cellular internalization in SK-BR-3 cells overexpressing the HER2 receptors (Figures A and B).

Table 2 Average loading efficiency and entrapment efficiency of studied formulations for DOX and Sili

Formulation	EE (%)		LE (%)	
	DOX	Sili	DOX	Sili
cGO-DOX	86.41 + 1.8	–	43.23 + 1.4	–
cGO-Sili	–	72.13 + 0.9	–	33.78 + 1.3
Apt-cGO-DOX	85.67 + 1.2	–	42.82 + 1.1	–
Apt-cGO-Sili	–	71.84 + 1.6	–	32.34 + 1.1
cGO-DOX-Sili	84.78 + 2.1	71.12 + 1.4	41.68 + 1.2	31.98 + 0.9
Apt-cGO-DOX-Sili	84.22 + 1.8	70.42 + 1.2	41.4 + 1.8	30.3 + 0.7

LE: loading efficiency; EE: entrapment efficiency; cGO: carboxylated graphene oxide; Apt: aptamer; DOX: doxorubicin; Sili: silibinin

Subsequently, the cellular internalization of free DOX, free Sili, mixed free drugs, and Apt-cGO-DOX-Sili was investigated using fluorescence microscopy based on the intrinsic green fluorescence of Sili and intrinsic red fluorescence of DOX. The blue fluorescence of DAPI was also utilized to label the nuclei of cancer cells. As depicted in Fig. 5C, when SK-BR-3 cells were exposed to free DOX and free Sili, the weak red and green fluorescence signals were accumulated in the nucleus and around the nucleus, respectively. Compared to free and mixed free drugs, when SK-BR-3 cells were exposed

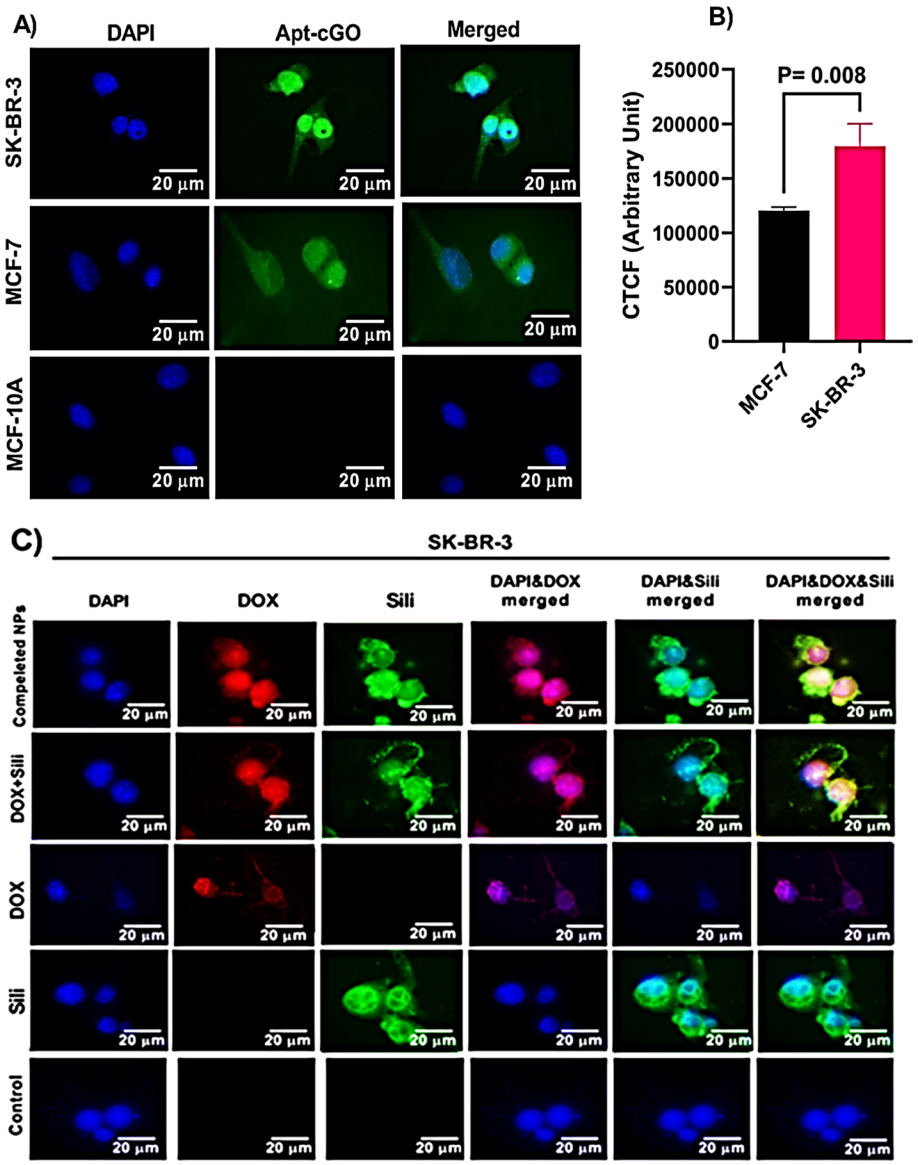

Fig. 5 **A** Cellular internalization of Apt-cGO into MCF-10A, SK-BR-3, and MCF-7 cells. **B** The quantification of cellular uptake capacity of Apt-cGO by calculating the CTCF. **C**, **D** The cellular internalization of DOX and Sili after the cell incubation with free DOX, free Sili, free DOX + free Sili, and completed NPs (Apt-cGO-DOX-Sili) for 3 h in SK-BR-3 cells (**C**) and MCF-7 cells (**D**). **E** The quantification of cellular uptake capacity of free DOX, free Sili, free DOX + free Sili, and completed NPs (Apt-cGO-DOX-Sili) by calculating the CTCF. The CTCF was calculated using Image J software. Data are provided as mean ± SD ($n = 3$). cGO: carboxylated Graphene oxide; Apt: aptamer; DOX: doxorubicin; Sili: silibinin; CTCF: corrected total cell fluorescence

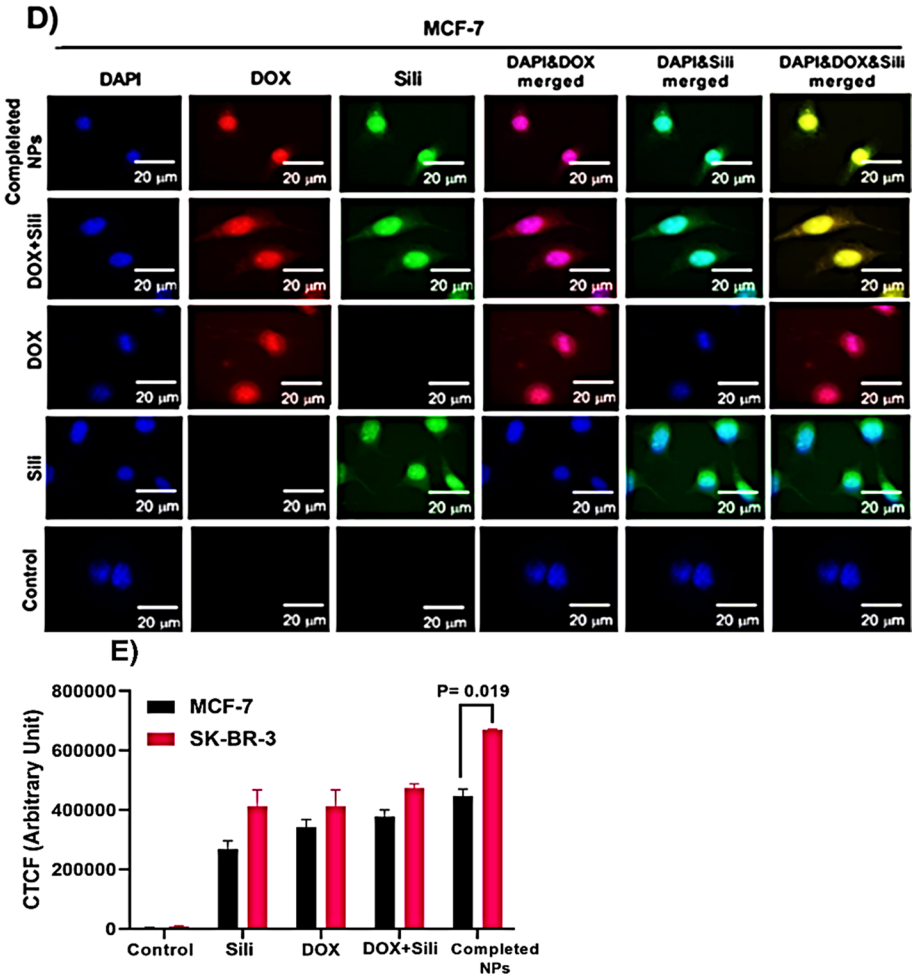

Fig. 5 continued

to Apt-cGO-DOX-Sili for 3 h, a larger amount of DOX red fluorescence and Sili green fluorescence were observed in the cells (Fig. 5C). Similar results were observed in MCF-7 cells (Fig. 5D). Compared to MCF-7, Apt-cGO-DOX-Sili delivered more DOX and Sili into SK-BR-3 cells, and the stronger red and green fluorescence were distributed in the SK-BR-3 cells (Fig. 5E).

In vitro drug release profiles

Temperature and pH-responsive systems have been attracted considerable attentions in the drug delivery applications and cancer treatment. Previous studies implied that the rate of drug release from nanocarriers could be controlled in response to different stimuli, such as temperature and pH. The acidic tumor microenvironment (pH ~ 6.5), which primarily results from the lactate production from anaerobic glycolysis, has been considered as a major feature of solid tumors. At the cellular level, the endosomes (pH ~ 5.5) and lysosomes (pH ~ 5.0) can also be involved in the promotion of drug release into the cytoplasm. In addition, drug release can also govern by variation in the environment temperature. Compared to healthy tissues (37 °C), tumor environment has a temperature greater (~ 40–42 °C), which is dependent on higher their metabolic activity and

vascularization. In addition, the thermos- and pH-sensitive drug release may help the minor release of drugs from nanocarriers under physiological conditions (pH 7.4, 37 °C) and decrease toxicity to the normal cells (Su and Kang 2020). According to this view, the in vitro release behavior of DOX and Sili from Apt-cGO was determined in the endosomal (pH 5.5, 42 °C) and the physiological conditions (pH 7.4, 37 °C) over a period of 72 h.

The in vitro release profile in Figs. 6A–D revealed the biphasic diffusion of DOX and Sili from nanocomposites with a burst initial release within 6 h, followed by sustained drug release for up to 72 h. The rate of DOX and Sili released from nanocomposites strongly depends on the medium's temperature and pH. Figure 6A, B exhibits much faster DOX release at pH 5.5 and 42 °C than at pH 7.4 and 37 °C. At the end of 72 h, about 64% and 68.2% of DOX were released from cGO-drug and Apt-cGO-drug in the tumor cells (pH 5.5 and 42 °C), respectively. At the same time, the cGO-drug and Apt-cGO-drug nanocomposites showed a similar release profile, as depicted in Fig. 6C, D. The cGO-drug and Apt-cGO-drug nanocomposites released about 66% and 70.2% of loaded Sili in tumor cells (pH 5.5 and 42 °C), respectively.

These results implied that the release of Sili and DOX from nanocomposites was facilitated in a temperature and pH-dependent manner. DOX and Sili could be cleaved from the Apt-cGO-DOX-Sili and subsequently diffused into the cytosol and later into the nucleus, enhancing the cell cytotoxicity. Under the thermal- and pH condition inside tumor cells, the $\pi \rightarrow \pi^*$ bonds and the amine groups of drugs are weakened and protonated, respectively (Motlagh et al. 2020). Collectively, these findings demonstrated that our engineered nanocomposite provides a platform to simultaneously release multiple

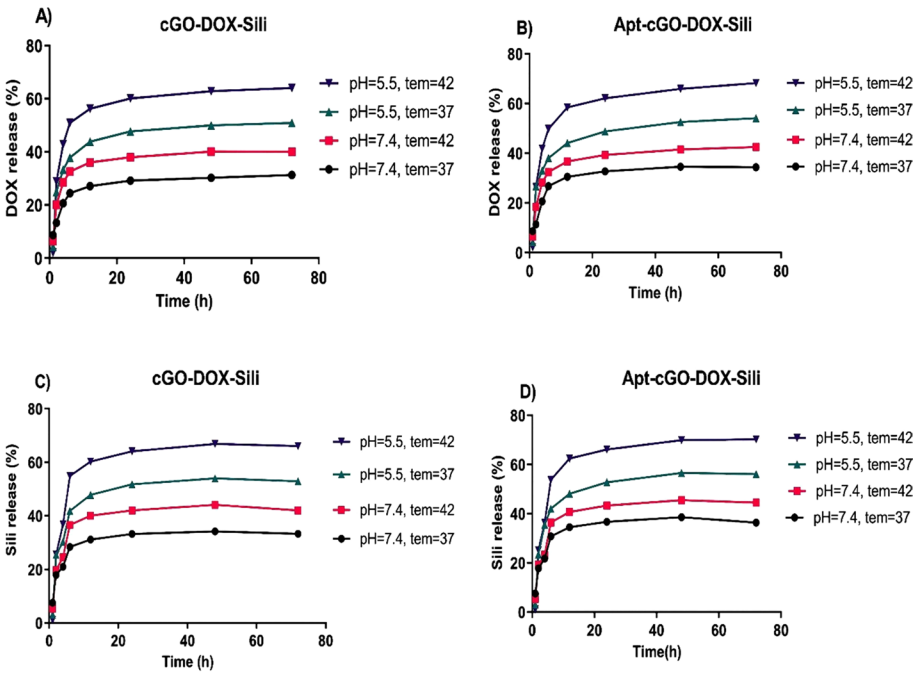

Fig. 6 **A**–**D** Are in vitro DOX and Sili release curves from cGO-DOX-Sili and Apt-cGO-DOX-Sili in different pH (pH 5.5 and pH 7.4) and temperatures (42 °C and 37 °C). cGO: carboxylated graphene oxide; Apt: aptamer; DOX: doxorubicin; Sili: silibinin

therapeutic drugs under thermos- and acidic conditions. The release profiles of cGO-drugs and Apt-cGO-drugs were virtually similar, indicating that the aptamer decoration on the surface of cGO nanosheets does not affect the drug release rate. At the same time, it enhances cellular internalization, causing better therapeutic efficiency.

In vitro cytotoxicity and synergistic effects of DOX and Sili

Extensive evidence verified that employing an effective delivery system for carrying chemotherapeutic drugs enhances their toxic effects in the target cancer cells (Yao et al. 2020). In previous work, Li et al. implied that the cytotoxicity of DOX-loaded NPs against breast cancer cells was enhanced noticeably compared to free DOX (Li et al. 2020). To inquire about the anticancer activity of our designed nanocomposites, the cytotoxicity effect of various formulations was examined against breast cancer cells (MCF-7 and SK-BR-3) and non-cancerous breast epithelial cells (MCF-10A) for an incubation period of 48 h. Figure 7A, andB illustrates the viability of MCF-10A, MCF-7, and SK-BR-3 cell under Apt and bare cGO exposure at various concentrations. As shown in Fig. 7A, and B, bare cGO and Apt did not show obvious cytotoxicity on cancerous and non-cancerous cells, which verified the biocompatibility of Apt-cGO. Subsequently, the cell toxicity of free drugs and drugs-conjugated nanocomposites were presented in Figs. 7C–I. According to MTT data analyses, free DOX and free Sili showed significant cytotoxicity against cancer and non-cancer cells in a dose-dependent manner after incubation for 48 h (Fig. 7C, andD). Compared to free drugs, cGO-drug (cGO-DOX and cGO-Sili) and Apt-cGO-drug (Apt-cGO-DOX and Apt-cGO-Sili), nanocomplexes exhibited substantially higher cytotoxicity on MCF-7 and SK-BR-3 cells (Figs. 7E–H). Besides, Apt-cGO-DOX-Sili nanocomposites represented the highest cytotoxicity on both breast cancer cell lines (Fig. 7I). The highest cytotoxicity reaction of Apt-cGO-DOX-Sili may be caused by better internalization of DOX and Sili by cancer cells relative to the other groups. Compared to MCF-7 cells, SK-BR-3 cells were more sensitive to Apt-cGO-DOX-Sili nanocomposites, probably due to the higher expression of the HER-2 protein as the HB5 receptor on the surface of SK-BR-3 cells (Liu et al. 2012). However, different nanocomplexes loaded with the Sili and DOX retain their safety characteristics on normal cells, with viability percentages exceeding 80% at each measured concentration.

The IC50 values of all formulations are provided in Table 3. In both cell lines, the IC50 values of Apt-cGO-DOX and Apt-cGO-Sili were lower than free DOX and free Sili, respectively, indicating the effective dose of Sili and DOX in the form of nanoparticles. Besides, the effective dose of DOX and Sili on the cell death of SK-BR-3 cells in the Apt-cGO-DOX-Sili form was less than the effective dose of other formulations. In addition, in the combined form of DOX and Sili, SK-BR-3 cells had a lower IC50 value compared to the MCF-7 cells (Table 3; $p < 0.0001$).

The results obtained from Compusyn software in both MCF-7 and SK-BR-3 cell lines showed that the CI level (Fa = 0.5) for dox + slb was above 1, and when they were loaded in nanoparticles, it was below 1. This finding suggested that the simple combination of DOX and Sili in the Apt-cGO nanoparticles causes synergistic effects of the two compounds and an obvious enhanced anti-tumor effect. In addition, the information from

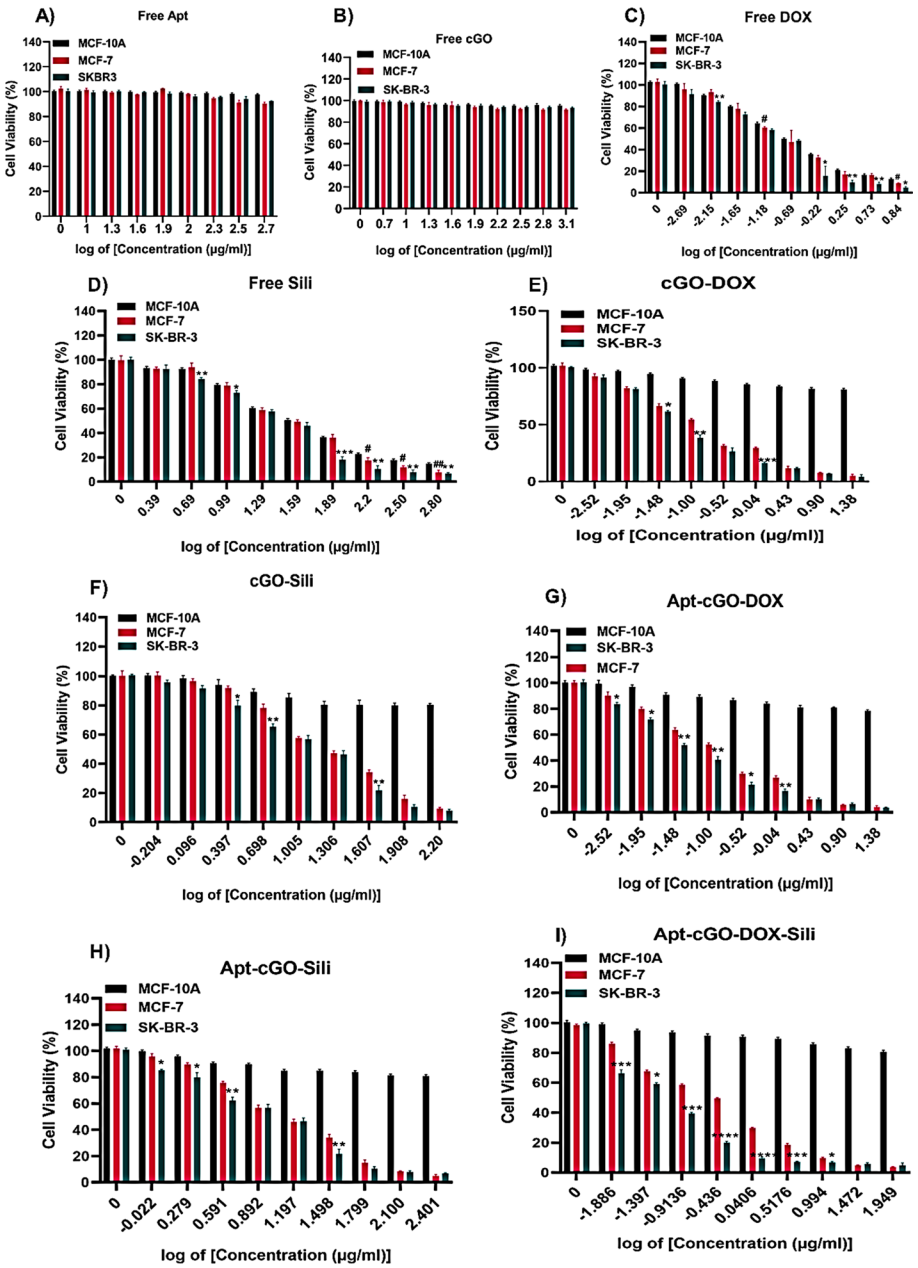

Fig. 7 Cytotoxicity of Free Apt (**A**), cGO (**B**), free DOX (**C**), free Sili (**D**), cGO-DOX (**E**), cGO-Sili (**F**), Apt-cGO-DOX (**G**), Apt-cGO-Sili (**H**), and Apt-cGO-DOX-Sili (**I**) on the MCF-10A, SK-BR-3, and MCF-7 cells in 48 h. The values are provided as mean ± SD ($n = 3$). $^{*}p < 0.05$, $^{**}p < 0.01$, $^{***}p < 0.001$, $^{****}p < 0.0001$ vs MCF-7 cells. $^{\#}p < 0.05$ and $^{\#\#}p < 0.01$ vs MCF-10A cells. cGO: carboxylated graphene oxide; Apt: aptamer; DOX: doxorubicin; Sili: silibinin

Compusyn software revealed that the linear correlation coefficient (r) in SKBR3 and MCF-7 cell lines was −0.9548 and −0.9966, respectively, which indicated that Apt-cGO-DOX-Sili is a very good model for drug delivery.

In vitro effects of Apt-cGO-DOX-Sili on cancer cell survival-related growth factors

At a molecular level, breast cancer is regulated by various intracellular growth factors and signals, of which PI3K/Akt is a prominent one. In HER2-positive breast cancer

Table 3 IC50 values of studied formulations toward MCF-7 and SK-BR-3 after 48 h

	IC50 values (log of [μg/mL])		*p*-value
	SK-BR-3	MCF-7	
Free Sili	1.42 + 0.09	1.581 + 0.1	0.021
cGO-Sili	1.097 + 0.09	1.252 + 0.2	0.792
Apt-cGO-Sili	0.963 + 0.05	1.108 + 0.1	0.14
Free DOX	− 0.712 + 0.06	− 0.761 + 0.1	0.961
cGO-DOX	− 1.163 + 0.09	− 0.899 + 0.01	0.004
Apt-cGO-DOX	− 1.239 + 0.05	− 0.999 + 0.02	0.005
Apt-cGO-DOX-Sili	− 1.329 + 0.08	− 0.613 + 0.01	< 0.0001

cells, high activation of PI3K/Akt/mTOR signaling pathway and its downstream factors, such as NF-κB, occurs in breast cancer, potentially implicated in the modulation of cell growth, cell metabolism, and apoptosis (Miricescu et al. 2020). Previous studies described the ability of flavonoids, such as silibinin, and conventional anticancer drugs, such as DOX, to block the PI3/AKT/mTOR pathway in various cancers (Raina et al. 2013; Shahidi et al. 2022c). However, combination strategies are employed to block cancer-related cell growth signaling pathways more effectively, mainly mediated by PI3K/AKT/mTOR pathway (Peng et al. 2022). Therefore, the current study analyzed the impact of Apt-cGO-DOX-Sili nanocomposites on the transcript levels of Akt, mTOR, and NF-κB genes. As shown in Fig. 8A–C, free drugs attenuated the transcript levels of Akt, mTOR, and NF-κB genes in both SK-BR-3 and MCF-7 cells ($p < 0.05$; $p < 0.01$; $p < 0.001$). Compared to free drugs, cGO-DOX and cGO-Sili complexes exhibited substantially higher inhibitory effects on the expression of target genes ($p < 0.01$; $p < 0.001$; $p < 0.0001$). Besides, Apt-cGO-DOX + Sili nanocomposites tagged with Apt showed the highest inhibitory effects on the transcript levels of Akt, mTOR, and NF-κB genes in both breast cancer cell lines ($p < 0.001$; $p < 0.0001$). Compared to MCF-7 cells, SK-BR-3 cells were more sensitive to the effects of Apt-cGO-DOX-Sili nanocomposites. We also exhibited similar changes in the transcript levels of CDK2 (Fig. 9A) as a downstream molecule in the PI3K/AKT/NF-kB signaling. CDK2 is identified as a major member of cell cycle components, which regulates G1 to S phase transitions through the phosphorylation of target genes (Ding et al. 2020).

The cascade of PI3K/Akt/mTOR is modulated by various cell regulators, such as cell cycle mediators. Rb is one of the well-characterized tumor suppressors that regulates G1/S transition by inhibiting the expression of the E2F family of transcription factors, leading to G1/S arrest. In addition, Rb can directly block the function of mTOR and increase sensitivity to chemotherapeutic agents (Knudsen et al. 2019). The Rb protein's deregulation frequently occurs in several human cancers, leading to elevated mTOR function and chemotherapeutic drug resistance (Zhang et al. 2016). To investigate the effect of our design nanocomposite on the Rb level, the transcript levels of Rb were determined, and the findings are provided in Fig. 9B. All formulations remarkably enhanced the transcript levels of Rb in SK-BR-3 and MCF-7 cells ($p < 0.05$; $p < 0.01$; $p < 0.001$; $p < 0.001$). As shown in Fig. 9B, Apt-cGO-DOX-Sili shows a higher Rb level than other formulations in SK-BR-3 and MCF-7 cells ($p < 0.001$; $p < 0.0001$).

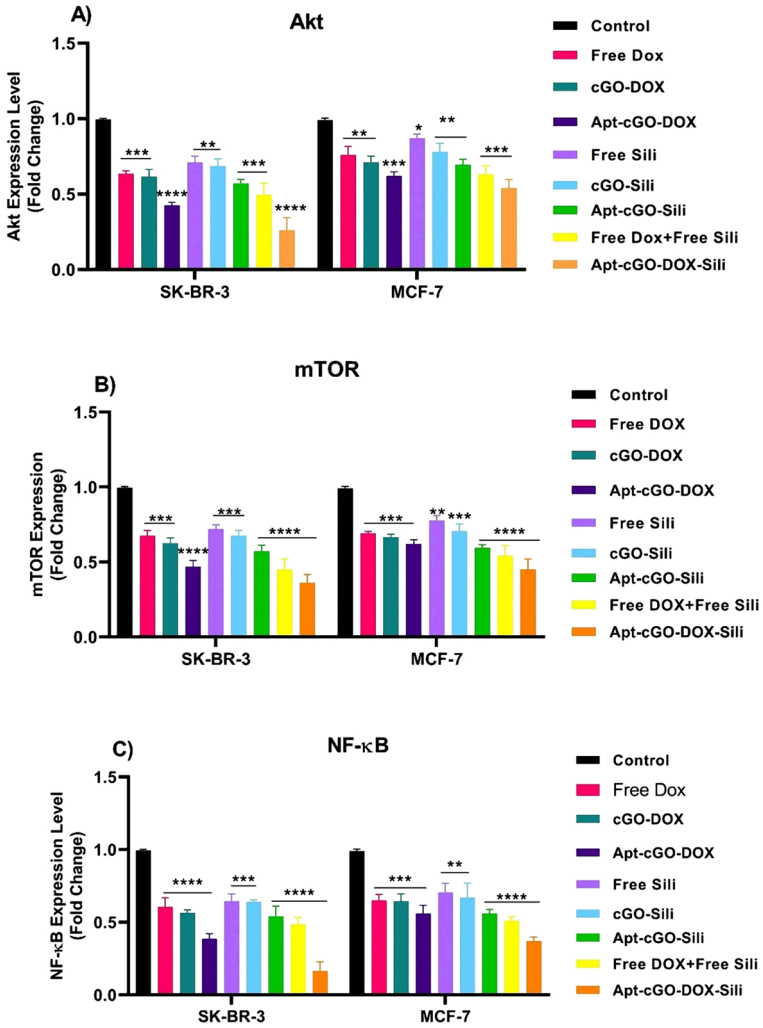

Fig. 8 The gene expression analysis of Akt (**A**), mTOR (**B**), and NF-κB (**C**) genes in SK-BR-3 and MCF-7 cells using the RT-qPCR technique. The analyzed values are reported as mean ± SD. ($n = 3$), $^{*}p < 0.05$, $^{**}p < 0.01$, $^{***}p < 0.001$, $^{****}p < 0.0001$ vs control. cGO: carboxylated graphene oxide; Apt: aptamer; DOX: doxorubicin; Sili: silibinin

In addition, we also investigated the effect of the designed Apt-cGO-DOX-Sili on the protein levels of CDK2 and Rb markers. As demonstrated in Fig. 9C–F, the incubation of cancer cells with free DOX resulted in an obvious increase in the expression of Rb protein and a notable decrease in the expression of CDK2 protein ($p < 0.05$). Compared to free DOX, cGO-DOX and Apt-cGO-DOX revealed a stronger impact on Rb and CDK2 protein levels ($p < 0.01$; $p < 0.001$). However, Apt-cGO-DOX-Sili exhibited the strongest effect relative to other formulations ($p < 0.001$). These findings show that simultaneous loading of Sili with DOX synergically enhances the anticancer effect of DOX.

Apoptosis analysis in MCF-7 and SK-BR-3 cells

The potential of cancer cells to evade apoptosis is proven as one of the cancer hallmarks (Sharma et al. 2019). Here, we determined the effect of Apt-cGO-DOX-Sili nanocomposites on the apoptosis rate in MCF-7 and SK-BR-3 cells. As depicted in

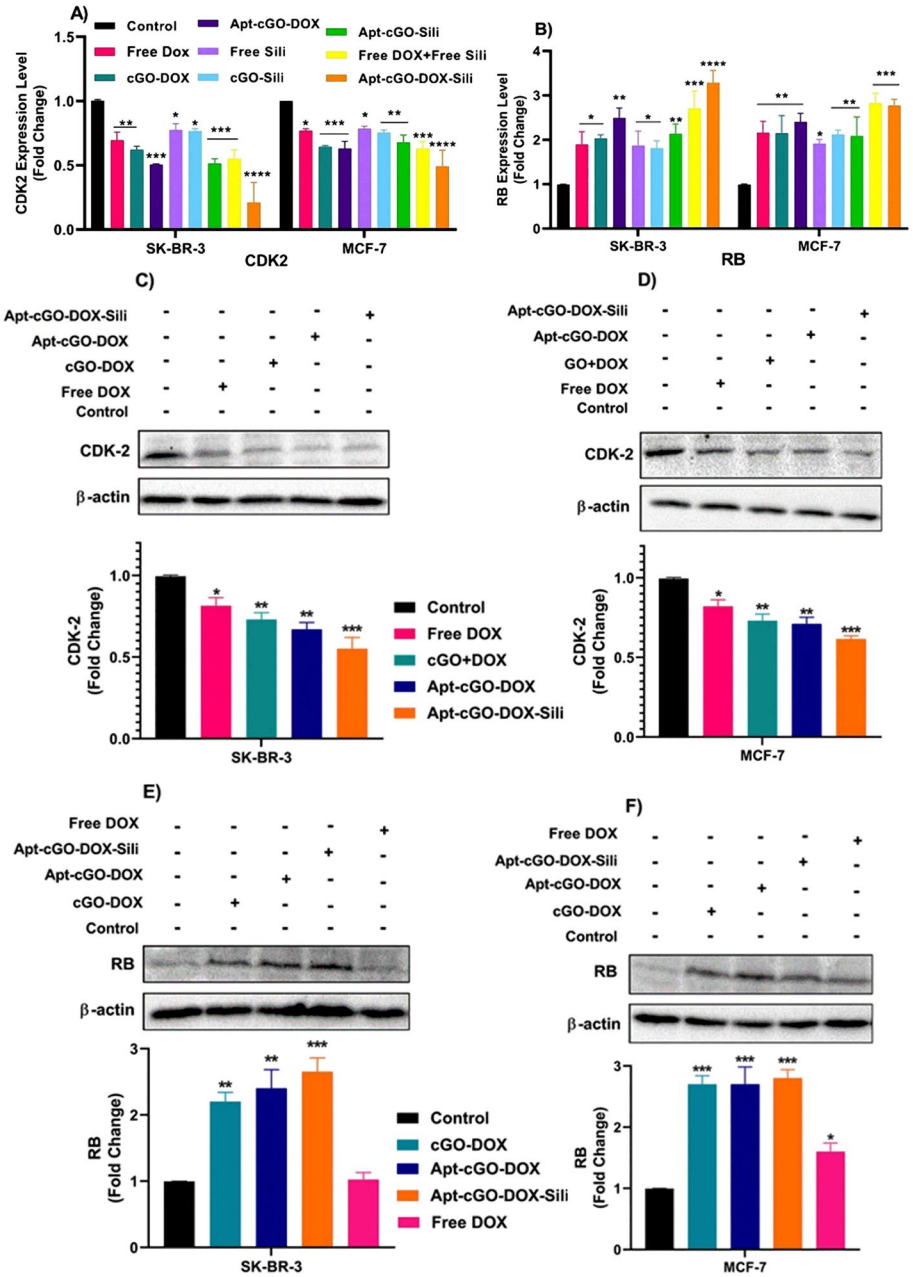

Fig. 9 Gene expression analysis of CDK2 (**A**) and Rb (**B**) genes in SK-BR-3 and MCF-7 cells using the RT-qPCR technique. The protein expression of CDK (**C**, **D**) and Rb (**E**, **F**) in SK-BR-3 and MCF-7 cells using western blot analysis. The analyzed values are shown as mean ± SD. ($n = 3$), $^{*}p < 0.05$, $^{**}p < 0.01$, $^{***}p < 0.001$, $^{****}p < 0.0001$ vs control. cGO: carboxylated graphene oxide; Apt: aptamer; DOX: doxorubicin; Sili: silibinin

Fig. 10A, and B, free drugs induced apoptosis rates in the breast cancer cells. The cGO-drug and Apt-cGO-drug were more potent in triggering apoptosis than the individual Sili and DOX. Besides, MCF-7 and SK-BR-3 cells exposed to Apt-cGO-DOX-Sili showed the highest apoptosis rate, which was in agreement with the obtained results in Figs. 8 and 9. Compared to MCF-7 cells, SK-BR-3 cells treated with Apt-cGO-DOX-Sili nanocomposites were more sensitive to apoptosis induction (Fig. 10C).

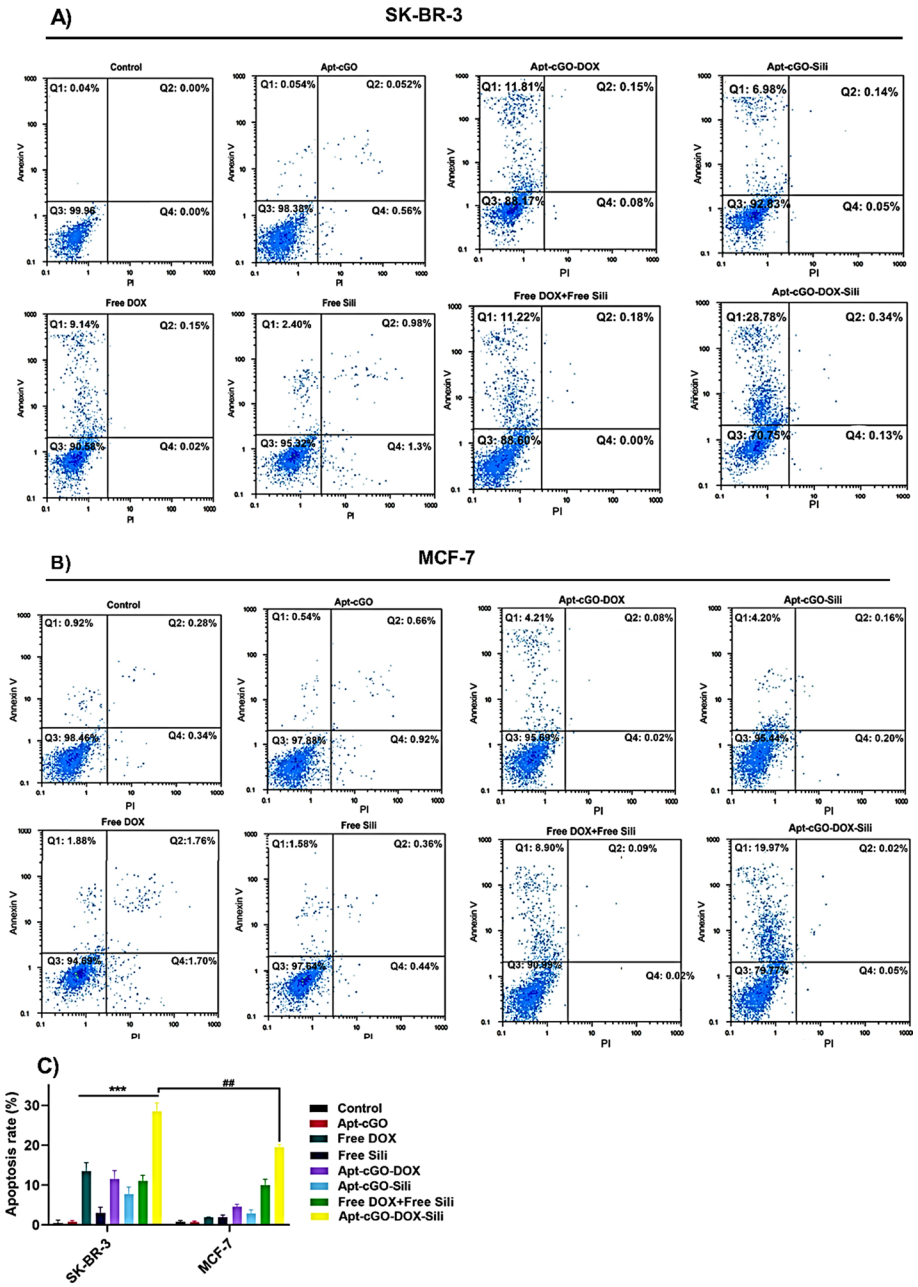

Fig. 10 Apoptosis rate analysis after SK-BR-3 (**A**) and MCF-7 (**B**) cells were exposed to different formulations for 48 h using flow cytometry. The flow cytometric charts indicate early apoptotic cells (Q1), late apoptotic cells (Q2), viable cells (Q3), and necrotic cells (Q4). **C** Comparative apoptotic rates between SK-BR-3 and MCF-7 cells exposed to different formulations for 48 h. The analyzed values are shown as mean ± SD. ($n = 3$). $^{***}p < 0.001$, $^{\#\#}p < 0.01$. cGO: carboxylated graphene oxide; Apt: aptamer; DOX: doxorubicin; Sili: silibinin

Conclusion

In this study, the aptamer-tagged cGO nanocarrier was successfully developed for co-delivering DOX and Sili (Apt-cGO-DOX-Sili) for effective breast cancer chemotherapy. The designed nanocarrier was nontoxic, as evaluated by a cell cytotoxicity study. Our findings revealed that the HB5 modification could recognize the

HER2-positive breast cancer cells and mediate selective cell uptake and cytotoxicity. Synergistic effects of Apt-cGO-DOX-Sili were seen, as in vitro increased cytotoxicity, decreased survival signals, and apoptosis induction in cancer cells. The co-loaded system exhibited a higher anticancer effect against SK-BR-3 cells than MCF-7 cells. These findings suggest that co-delivery of DOX and Sili by Apt-cGO-DOX-Sili might be a promising strategy for breast cancer therapy. However, in-vivo studies are needed to confirm the in vitro results.

Author contributions
MS, BFH and OA contributed to methodology, investigation and writing original draft. MH, PD, HZJ, NSHM, SMN and AM helped in writing original draft, writing-review, editing and validation. All authors read and approved the final manuscript.

Funding
The authors state no funding involved.

Availability of data and materials
The data sets generated during and/or analyzed during the current study are available from the corresponding author on reasonable request.

Declarations

Ethics approval and consent to participate
Not applicable.

Consent for publication
All authors agree to publication.

Competing interests
The authors state no conflict of interest.

Received: 26 October 2022 Accepted: 18 May 2023
Published online: 03 June 2023

References

Afzal M, Alharbi KS, Alruwaili NK, Al-Abassi FA, Al-Malki AAL, Kazmi I et al (2021) Nanomedicine in treatment of breast cancer—a challenge to conventional therapy. Semin Cancer Biol 69:279–292
Ali N, Teixeira JA, Addali A (2018) A review on nanofluids: fabrication, stability, and thermophysical properties. J Nanomater 2018:1–33
Alibolandi M, Mohammadi M, Taghdisi SM, Ramezani M, Abnous K (2017) Fabrication of aptamer decorated dextran coated nano-graphene oxide for targeted drug delivery. Carbohydr Polym 155:218–229
Alipour M, Reza Bigdeli M, Aligholi H, Rasoulian B, Khaksarian M (2020) Sustained release of silibinin-loaded chitosan nanoparticle induced apoptosis in glioma cells. J Biomed Mater Res Part A 108(3):458–469
Barbatti M, Ruckenbauer M, Szymczak JJ, Sellner B, Vazdar M, Antol I, et al. Model systems for dynamics of π-conjugated biomolecules in excited states. Handb. Comput. Chem. Springer, Netherlands; 2012;1175–214
Bustos-Ramírez K, Martínez-Hernández AL, Martínez-Barrera G, De Icaza M, Castaño VM, Velasco-Santos C (2013) Covalently bonded chitosan on graphene oxide via redox reaction. Materials 6(3):911–926
Chandra S, Nguyen HM, Wiltz K, Hall N, Chaudhry S, Olverson G et al (2020) Aptamer-functionalized hybrid nanoparticles to enhance the delivery of doxorubicin into breast cancer cells by silencing P-glycoprotein. J Cancer Treat Diagnosis 4(1):1
Chen BW, Chen W, Liang H, Liu H, Liang C, Zhi X et al (2015) Inhibition of mTORC2 induces cell-cycle arrest and enhances the cytotoxicity of doxorubicin by suppressing MDR1 expression in HCC CellsmTORC2 inhibition enhances the cytotoxicity of doxorubicin. Mol Cancer Ther 14(8):1805–1815
Chou T-C (2010) Drug combination studies and their synergy quantification using the Chou-Talalay method synergy quantification method. Cancer Res 70(2):440–446
Dasari Shareena TP, McShan D, Dasmahapatra AK, Tchounwou PB (2018) A review on graphene-based nanomaterials in biomedical applications and risks in environment and health. Nano-Micro Lett 10(3):1–34
Ding L, Cao J, Lin W, Chen H, Xiong X, Ao H et al (2020) The roles of cyclin-dependent kinases in cell-cycle progression and therapeutic strategies in human breast cancer. Int J Mol Sci 21(6):1960
Esmaeili Y, Bidram E, Zarrabi A, Amini A, Cheng C (2020) Graphene oxide and its derivatives as promising In-vitro bio-imaging platforms. Sci Rep 10(1):1–13
Firouzi Amoodizaj F, Baghaeifar S, Taheri E, Farhoudi Sefidan Jadid M, Safi M, Seyyed Sani N et al (2020) Enhanced anticancer potency of doxorubicin in combination with curcumin in gastric adenocarcinoma. J Biochem Mol Toxicol 34(6):e22486

Ghalehkhondabi V, Soleymani M, Fazlali A (2021) Folate-targeted nanomicelles containing silibinin as an active drug delivery system for liver cancer therapy. J Drug Deliv Sci Technol 61:102157
Gholami A, Emadi F, Nazem M, Aghayi R, Khalvati B, Amini A et al (2020) Expression of key apoptotic genes in hepatocellular carcinoma cell line treated with etoposide-loaded graphene oxide. J Drug Deliv Sci Technol 57:101725
Ghulam AN, Dos Santos OAL, Hazeem L, Pizzorno Backx B, Bououdina M, Bellucci S (2022) Graphene oxide (GO) materials—applications and toxicity on living organisms and environment. J Funct Biomater 13(2):77
Guo S, Raya J, Ji D, Nishina Y, Ménard-Moyon C, Bianco A (2020) Is carboxylation an efficient method for graphene oxide functionalization? Nanoscale Adv. 2(9):4085–4092
Hummers WS Jr, Offeman RE (1958) Preparation of graphitic oxide. J Am Chem Soc 80(6):1339
Karimi R, Bakhshi A, Dayati P, Abazari O, Shahidi M, Savaee M et al (2022) Silymarin reduces retinal microvascular damage in streptozotocin-induced diabetic rats. Sci Rep 12(1):1–14
Kim HJ, Park JY, Lee TS, Song IH, Cho YL, Chae JR et al (2019) PET imaging of HER2 expression with an 18F-fluoride labeled aptamer. PLoS ONE 14(1):e0211047
Knudsen ES, Pruitt SC, Hershberger PA, Witkiewicz AK, Goodrich DW (2019) Cell cycle and beyond: exploiting new RB1 controlled mechanisms for cancer therapy. Trends in Cancer 5(5):308–324
Kruger NJ. The Bradford method for protein quantitation. Protein Protoc. Handb. Springer; 2009;17–24.
Li W-G, Wang H-Q (2016) Inhibitory effects of Silibinin combined with doxorubicin in hepatocellular carcinoma; an in vivo study. J BUON 21(4):917–924
Li R, Guiney LM, Chang CH, Mansukhani ND, Ji Z, Wang X et al (2018) Surface oxidation of graphene oxide determines membrane damage, lipid peroxidation, and cytotoxicity in macrophages in a pulmonary toxicity model. ACS Nano 12(2):1390–1402
Li J, Li M, Tian L, Qiu Y, Yu Q, Wang X et al (2020) Facile strategy by hyaluronic acid functional carbon dot-doxorubicin nanoparticles for CD44 targeted drug delivery and enhanced breast cancer therapy. Int J Pharm 578:119122
Liu Z, Duan J-H, Song Y-M, Ma J, Wang F-D, Lu X et al (2012) Novel HER2 aptamer selectively delivers cytotoxic drug to HER2-positive breast cancer cells in vitro. J Transl Med 10(1):1–10
Liu C, Ma X, Zhuang J, Liu L, Sun C (2020) Cardiotoxicity of doxorubicin-based cancer treatment: what is the protective cognition that phytochemicals provide us? Pharmacol Res 160:105062
Ma F, Nian J, Bi C, Yang M, Zhang C, Liu L et al (2019) Preparation of carboxylated graphene oxide for enhanced adsorption of U (VI). J Solid State Chem 277:9–16
Malik MT, O'Toole MG, Casson LK, Thomas SD, Bardi GT, Reyes-Reyes EM et al (2015) AS1411-conjugated gold nanospheres and their potential for breast cancer therapy. Oncotarget 6(26):22270
Miricescu D, Totan A, Stanescu-Spinu I-I, Badoiu SC, Stefani C, Greabu M (2020) PI3K/AKT/mTOR signaling pathway in breast cancer: from molecular landscape to clinical aspects. Int J Mol Sci 22(1):173
Motlagh NSH, Parvin P, Mirzaie ZH, Karimi R, Sanderson JH, Atyabi F (2020) Synergistic performance of triggered drug release and photothermal therapy of MCF7 cells based on laser activated PEGylated GO+ DOX. Biomed Opt Express 11(7):3783–3794
Nawaz Q, Fuentes-Chandia M, Tharmalingam V, Rehman MAU, Leal-Egana A, Boccaccini AR (2020) Silibinin releasing mesoporous bioactive glass nanoparticles with potential for breast cancer therapy. Ceram Int 46(18):29111–29119
Patel A, Unni N, Peng Y (2020) The changing paradigm for the treatment of HER2-positive breast cancer. Cancers 12(8):2081
Patra JK, Das G, Fraceto LF, Campos EVR, del Pilar R-T, Acosta-Torres LS et al (2018) Nano based drug delivery systems: recent developments and future prospects. J Nanobiotechnol 16(1):1–33
Peng Y, Wang Y, Zhou C, Mei W, Zeng C (2022) PI3K/Akt/mTOR pathway and its role in cancer therapeutics: are we making headway? Front Oncol 12:819128
Pooja D, Bikkina DJB, Kulhari H, Nikhila N, Chinde S, Raghavendra YM et al (2014) Fabrication, characterization and bioevaluation of silibinin loaded chitosan nanoparticles. Int J Biol Macromol 69:267–273
Pooresmaeil M, Javanbakht S, Nia SB, Namazi H (2020) Carboxymethyl cellulose/mesoporous magnetic graphene oxide as a safe and sustained ibuprofen delivery bio-system: synthesis, characterization, and study of drug release kinetic. Colloids Surf A Physicochem Eng Asp 594:124662
Pourgholi A, Dadashpour M, Mousapour A, Amandi AF, Zarghami N (2021) Anticancer potential of silibinin loaded polymeric nanoparticles against breast cancer cells: insight into the apoptotic genes targets. Asian Pac J Cancer Prev 22(8):2587
Raina K, Agarwal C, Wadhwa R, Serkova NJ, Agarwal R (2013) Energy deprivation by silibinin in colorectal cancer cells: a double-edged sword targeting both apoptotic and autophagic machineries. Autophagy 9(5):697–713
Senapati S, Mahanta AK, Kumar S, Maiti P (2018) Controlled drug delivery vehicles for cancer treatment and their performance. Signal Transduct Target Ther 3(1):1–19
Shahidi M, Abazari O, Bakhshi A, Zavarreza J, Modarresi M, Haghiralsadat F et al (2022) Multicomponent siRNA/miRNA-loaded modified mesoporous silica nanoparticles targeted bladder cancer for a highly effective combination therapy. Front Bioeng Biotechnol 1(10):949704
Shahidi M, Abazari O, Dayati P, Bakhshi A, Rasti A, Haghiralsadat F et al (2022b) Aptamer-functionalized chitosan-coated gold nanoparticle complex as a suitable targeted drug carrier for improved breast cancer treatment. Nanotechnol Rev 11(1):2875–2890
Shahidi M, Moradi A, Dayati P (2022c) Zingerone attenuates zearalenone-induced steroidogenesis impairment and apoptosis in TM3 Leydig cell line. Toxicon 211:50–60
Sharma A, Boise LH, Shanmugam M (2019) Cancer metabolism and the evasion of apoptotic cell death. Cancers 11(8):1144
Shetty PK, Manikkath J, Tupally K, Kokil G, Hegde AR, Raut SY et al (2017) Skin delivery of EGCG and silibinin: potential of peptide dendrimers for enhanced skin permeation and deposition. AAPS PharmSciTech 18(6):2346–2357
Shrestha S, Wang B, Dutta P (2020) Nanoparticle processing: understanding and controlling aggregation. Adv Colloid Interface Sci 279:102162

Si L, Liu W, Hayashi T, Ji Y, Fu J, Nie Y et al (2019) Silibinin-induced apoptosis of breast cancer cells involves mitochondrial impairment. Arch Biochem Biophys 671:42–51
Solís-Gómez A, Sato-Berrú RY, Mata-Zamora ME, Saniger JM, Guirado-López RA (2019) Characterizing the properties of anticancer silibinin and silybin B complexes with UV–Vis, FT-IR, and Raman spectroscopies: a combined experimental and theoretical study. J Mol Struct 1182:109–118
Song S, Shen H, Wang Y, Chu X, Xie J, Zhou N et al (2020) Biomedical application of graphene: from drug delivery, tumor therapy, to theranostics. Colloids Surf B Biointerfaces 185:110596
Song G, Shui R, Wang D, Fang R, Yuan T, Li L et al (2022) Aptamer-conjugated graphene oxide-based surface assisted laser desorption ionization mass spectrometry for selective extraction and detection of Aβ1–42 in an Alzheimer's disease SH-SY5 cell model [Internet]. Front Aging Neurosci. Available from:https://www.frontiersin.org/articles/10.3389/fnagi.2022.993281
Su S, Kang PM (2020) Recent advances in nanocarrier-assisted therapeutics delivery systems. Pharmaceutics 12(9):837
Subramaniyan V, Fuloria S, Gupta G, Kumar DH, Sekar M, Sathasivam KV et al (2022) A review on epidermal growth factor receptor's role in breast and non-small cell lung cancer. Chem Biol Interact 351:109735
Sung H, Ferlay J, Siegel RL, Laversanne M, Soerjomataram I, Jemal A et al (2021) Global cancer statistics 2020: GLOBOCAN estimates of incidence and mortality worldwide for 36 cancers in 185 countries. CA Cancer J Clin 71(3):209–249
Tan J, Lai Z, Zhong L, Zhang Z, Zheng R, Su J et al (2018) A graphene oxide-based fluorescent aptasensor for the turn-on detection of CCRF-CEM. Nanoscale Res Lett 13(1):1–8
Tuli HS, Mittal S, Aggarwal D, Parashar G, Parashar NC, Upadhyay SK et al (2021) Path of Silibinin from diet to medicine: a dietary polyphenolic flavonoid having potential anti-cancer therapeutic significance. Semin Cancer Biol 73:196–218
van der Zanden SY, Qiao X, Neefjes J (2021) New insights into the activities and toxicities of the old anticancer drug doxorubicin. FEBS J 288(21):6095–6111
Varela-López A, Battino M, Navarro-Hortal MD, Giampieri F, Forbes-Hernández TY, Romero-Márquez JM et al (2019) An update on the mechanisms related to cell death and toxicity of doxorubicin and the protective role of nutrients. Food Chem Toxicol 134:110834
Wu X, Shaikh AB, Yu Y, Li Y, Ni S, Lu A et al (2017) Potential diagnostic and therapeutic applications of oligonucleotide aptamers in breast cancer. Int J Mol Sci 18(9):1851
Yadav S, Singh Raman AP, Meena H, Goswami AG, Bhawna, Kumar V et al (2022) An update on graphene oxide: applications and toxicity. ACS Omega 7:35387
Yan L, Shen J, Wang J, Yang X, Dong S, Lu S (2020) Nanoparticle-based drug delivery system: a patient-friendly chemotherapy for oncology. Dose-Response 18(3):1559325820936161
Yao Y, Zhou Y, Liu L, Xu Y, Chen Q, Wang Y et al (2020) Nanoparticle-based drug delivery in cancer therapy and its role in overcoming drug resistance. Front Mol Biosci 7:193
Yi G, Son J, Yoo J, Park C, Koo H (2018) Application of click chemistry in nanoparticle modification and its targeted delivery. Biomater Res. 22(1):1–8
Zhang J, Xu K, Liu P, Geng Y, Wang B, Gan W et al (2016) Inhibition of Rb phosphorylation leads to mTORC2-mediated activation of Akt. Mol Cell 62(6):929–942
Zhao X, Wei Z, Zhao Z, Miao Y, Qiu Y, Yang W et al (2018) Design and development of graphene oxide nanoparticle/chitosan hybrids showing pH-sensitive surface charge-reversible ability for efficient intracellular doxorubicin delivery. ACS Appl Mater Interfaces 10(7):6608–6617
Zhu G, Chen X (2018) Aptamer-based targeted therapy. Adv Drug Deliv Rev 134:65–78

Publisher's Note